Scientific Reports

https://doi.org/10.1038/s41598-026-60314-2

Article in Press

Planar neural organoids as an advanced *in vitro* model to study patient-derived melanoma metastasis

Received: 1 July 2025

Accepted: 26 June 2026

Published online: 03 July 2026

Cite this article as: Majumder J., Torr E.E., Favreau P.F. *et al.* Planar neural organoids as an advanced *in vitro* model to study patient-derived melanoma metastasis. *Sci Rep* (2026). https://doi.org/10.1038/s41598-026-60314-2

Joydeb Majumder, Elizabeth E. Torr, Peter F. Favreau, Apoorva Ramamurthy, Ulrika Müller, Grzegorz Sabat, Connie S. Lebakken & William L. Murphy

Planar Neural Organoids as an Advanced *In Vitro* Model to Study Patient-Derived Melanoma Metastasis

Joydeb Majumder[1], Elizabeth E. Torr[1], Peter F. Favreau[2], Apoorva Ramamurthy[1], Ulrika Müller[1], Grzegorz Sabat[3], Connie S. Lebakken[2], and William L. Murphy[1,4]*

[1]Department of Orthopedics and Rehabilitation, University of Wisconsin-Madison, Madison, WI-53705, USA

[2]Stem Pharm, Incorporated, Madison, WI-53711, USA

[3]Biotechnology Center, University of Wisconsin-Madison, Madison, WI-53706, USA

[4]Department of Biomedical Engineering, University of Wisconsin-Madison, Madison, WI-53705, USA

* Corresponding author E-mail address: wlmurphy@wisc.edu (W. L. Murphy)

Keywords: stem cells, PEG hydrogel, neural organoids, melanoma, brain metastasis

Abstract

Metastasis, which occurs when cancer cells spread from their original site in the body to other organs - is the leading cause of death in cancer patients. Conventional two-dimensional (2D) cell cultures along with orthotopic animal models are widely used to study and develop therapeutics for metastatic cancers. However, 2D cell cultures do not accurately reflect the physiology of real tissues, and the results obtained from the orthotopic animal models cannot always be applied to humans due to the interspecies differences. The recent emergence of human organoid models provides unique opportunities to study the complex cellular interactions in a near-physiological 3D environment. In this study, we have engineered an *in vitro* melanoma metastasis model using patient-derived melanoma cells and human-induced pluripotent stem cells (iPSCs)-derived planar neural organoids (PNOs). We investigated metastatic cancer processes such as the growth of melanoma

cells, and evaluated the effects of anti-cancer drug treatment on it. Our results demonstrated that the 3D PNO system served as a more effective *in vitro* model than conventional 2D cultures to study melanoma brain metastases, and this PNO system can also be used to model other types of poorly understood metastatic cancers under physiological environments.

Introduction

Metastasis refers to the process in which cancer cells disseminate from the original tumor site, migrate through the lymph system, and form a new tumor in other organs in the body.[1] Brain metastases, which occur when cancer cells spread to the brain from an initial tumor site in the body, are one of the leading causes of mortality of patients with cancer.[2] Despite advancements in cancer treatment, the median survival duration of patients with brain metastases is less than six months.[3] Currently, 2D cancer cell cultures and orthotopic animal models are widely used methods to study and develop therapeutics for metastatic cancers.[4, 5] However, 2D cell cultures are limited by the absence of cell-microenvironment interactions,[6-10] pH gradients, [11, 12] and the accumulation of genomic alterations of cells after extended 2D culture.[13] Orthotopic animal models that include host-tumor cell interactions are the next conventional steps after 2D cell cultures. However, the results obtained from animal models often cannot be directly translated into human outcomes because of interspecies differences.[14] These limitations led to the development of 3D cell culture models that more closely mimic certain features of *in vivo* environments. In particular, the recent emergence of

human stem cell-derived organoid cultures provides opportunities for disease modeling in conditions that may be closer to the physiological environment. Organoids are self-assembled three-dimensional *in vitro* tissue constructs capable of showing certain organ-like characteristics. In recent years, researchers have developed organoids of the human brain [15-20], stomach [21-26], pancreas [27-31], colon [32-35], liver [36-42], and heart [43, 44] using various types of stem cells. Neural organoids are typically comprised of neural, astroglial, and vascular components that show structural or functional similarity to human neural tissues.[45] For example, we previously demonstrated assembly of planar neural organoids (PNOs) by adding human stem cell-derived neural progenitors, endothelial cells, pericytes, and microglia progenitors to a defined synthetic hydrogel and allowing for self-organization.[46-48] The resulting PNOs were sufficiently translucent to allow for longitudinal fluorescence imaging, and were grown in 96-well plate format that responded to lipopolysaccharide (LPS)-stimulated inflammation, and were responsive to clinically used anti-inflammatory drugs. [46]

In the current study, we used PNOs as a 3D *in vitro* model to study melanoma brain metastasis including melanoma cell incorporation, growth and drug response. Our results revealed that the melanoma cells obtained from patients were able to integrate and proliferate within PNOs, and that melanoma cell growth influenced the neural, vascular, and neuroinflammatory signaling within the organoids. Further, the melanoma cells growing within PNOs responded to the BRAF (B-Raf proto-oncogene)

inhibitor Dabrafenib (DAB) and MEK (mitogen-activated protein kinase) inhibitor Trametinib (TRA), which are clinically used anti-cancer agents to treat melanoma. Taken together, our results indicate that the human PNO model can provide a distinct human tissue context to study metastatic brain cancers and to screen for potential treatments.

Results and Discussion

Culture of melanoma cells within planar neural organoids

Culture of mCherry-positive melanoma cells within human iPSC-derived organoids led to the formation of planar neural organoids termed here as 'PNO-Mel' as compared to the PNOs without melanoma cells termed 'PNO.' Human iPSC-differentiated endothelial cells (iPSC-ECs), pericyte cells (iPSC-PCs), neural progenitor cells (iPSC-NPCs), and microglia (iPSC-MG) were added on the PEG hydrogel surface as schematically shown (Fig. 1A). Patient-derived melanoma cells 16-255 Mel and 11-743 Mel were seeded on top of the growing PNOs on day 14, and the co-culture of PNOs and melanoma was continued until day 28 in serum and antibiotic-free growth medium. We monitored the growth of the melanoma cell populations in the PNO over the period from day 14 to day 28 (Fig. 1B).

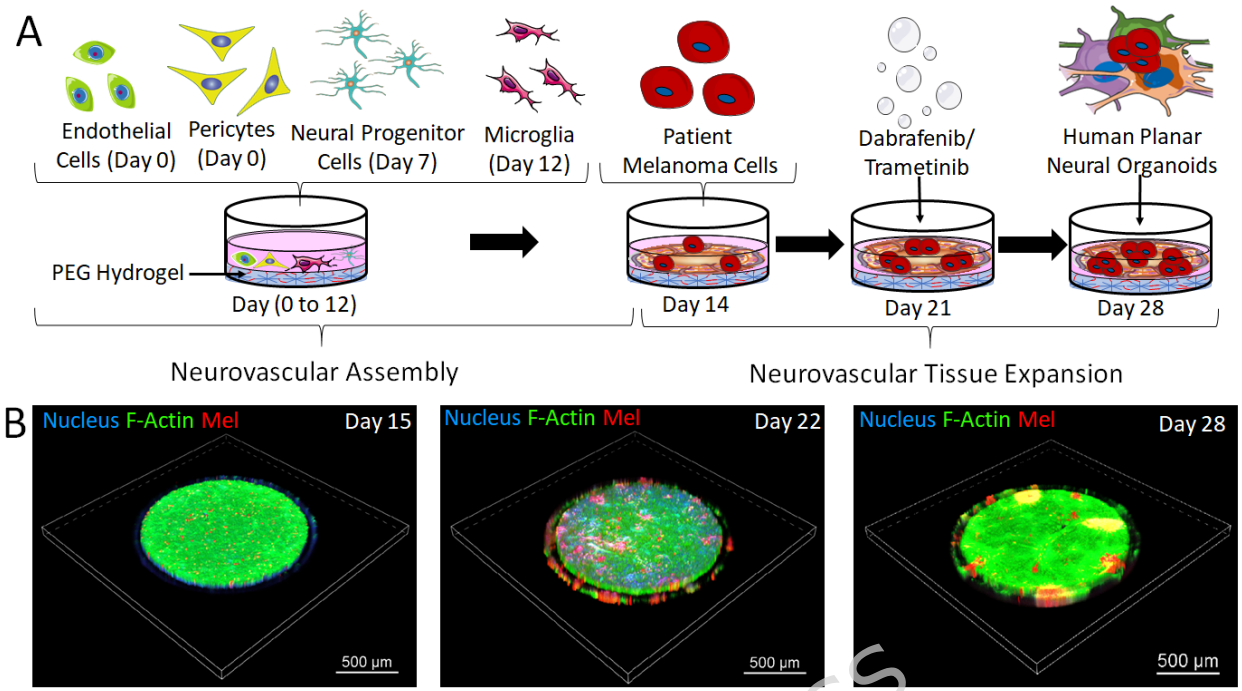

Fig. 1. Schematic and confocal images showing culture and expansion of human planar neural organoids, and seeding of patient melanoma cells. (A) Human induced pluripotent stem cells (iPSCs) derived precursor cells were co-cultured on the synthetic poly (ethylene glycol) (PEG) hydrogels in 96-well plates. Endothelial cells (ECs) and pericyte cells (PCs) were seeded at day 0, followed by the addition of neural progenitor cells (NPCs) on day 7 and microglia (MG) on day 12. Patient-derived mCherry-positive melanoma cell lines 16-255 Mel and 11-743 Mel were added to the neural organoids on day 14, and anti-cancer drugs (2 nM) were added daily starting on day 21. (B) Representative confocal microscopy images showing growth of the mCherry-positive 16-255 melanoma cells cultured within the neural organoids over time on Day 15, Day 22, and Day 28. Scale bar: 500 µm.

Confocal images showed substantially slower growth of the melanoma cells over time in the PNO system when compared to the growth of the melanoma cells on a conventional 2D plastic surface (Fig. 1B, Fig. S1-2). We also observed slower growth of the 11-743 Mel cells as compared to 16-255 Mel cells on the PNOs. Confocal microscopy images at day 28 showed that the

PNO-16-255 Mel tissue was thicker (211.00 ± 24.60 µm) when compared to either the PNO without melanoma cells (146.30 ± 15.90 µm) or the PNO-11-743 Mel (163.70 ± 21.60 µm) organoids (Fig. 2A-B, Fig. S3). This increased thickness could be due to the higher growth rate of the 16-255 Mel cells as compared to that of the 11-743 Mel cells in the organoids.

Characterization of neurovascular signals in the PNOs

PNO-Mel organoids showed less apparent vascular networks than those formed in PNOs. Confocal images showed the presence of the vascular marker protein (CD31) throughout the PNOs (Fig. 3A), and $CD31^+$ cells formed an interconnected network as shown in our previous studies. [46-48] In contrast, PNO-Mel showed an apparently less interconnected CD31 endothelial network (Fig. 3A). In addition, PNO-Mel produced lower levels of vascular endothelial growth factor (VEGF) when compared to PNOs (Fig. 3C). These findings suggest that the presence of melanoma cells may interfere with the formation of the vascular network in the PNOs.

Both the PNO and PNO-Mel samples showed the presence of the neuronal marker β3-tubulin, glutamatergic neuron marker VGLUT1, and cortical neuron marker CUX1 (Fig. 3B, Fig. S4); however more apparent interconnected CUX1 cortical neuronal networks were observed in the PNO than that in PNO-Mel organoids. The PNO-Mel also showed reduced production of brain-derived neurotrophic factor (BDNF) when compared to PNO (Fig. 3D), further suggesting that melanoma cell growth may interfere with the formation of neural networks within the PNO.

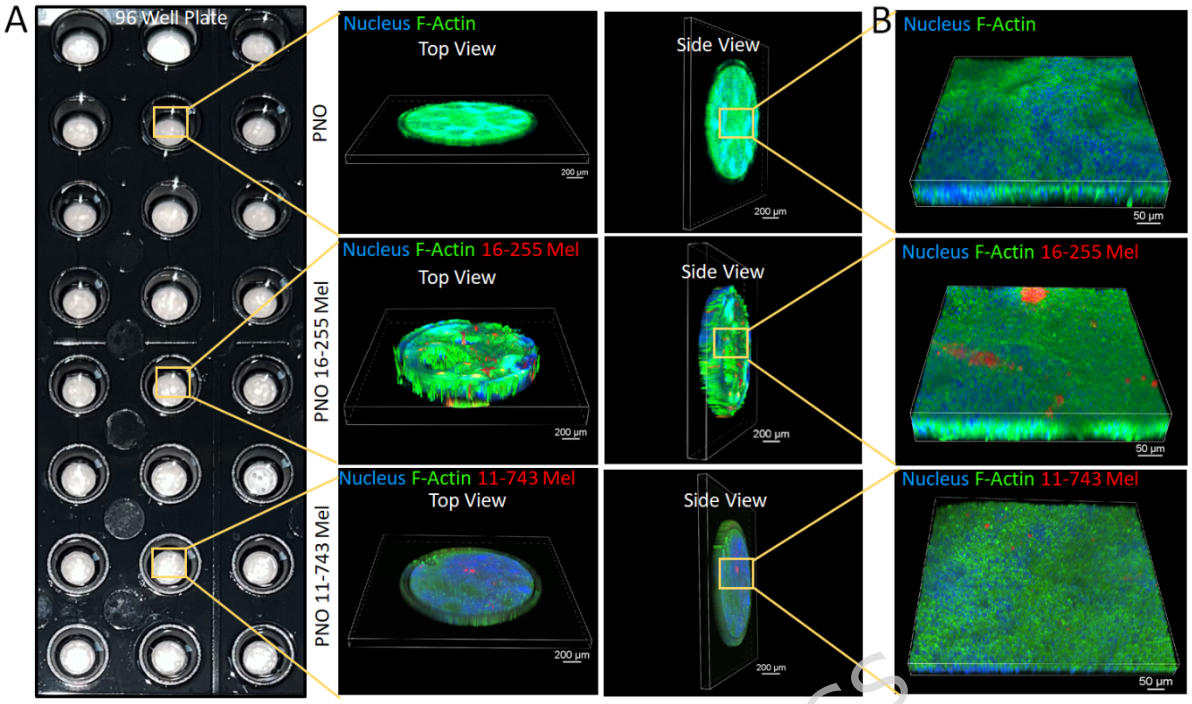

Fig. 2. Morphology of the planar neural organoids cultured with and without the addition of melanoma cells. (A) Macroscopic images of day 28 of the 96-well plate used in the organoid culture. (B) Microscopic images of day 28 of the planar neural organoids cultured with and without the mCherry-positive 16-255 or 11-743 melanoma cells.

Characterization of astrocyte and microglia signals in the PNOs

Expression of multiple microglia markers was higher in PNOs when compared to PNO-Mel organoids. Confocal images showed the presence of both the glial marker Glial Fibrillary Acidic Protein (GFAP) (Fig. 4A) and the microglial marker ‘ionized calcium binding adaptor molecule 1’ (IBA1) within PNO and PNO-Mel (Fig. 4B). Higher resolution confocal images showed more apparent expression of the microglia marker IBA1 within the PNO as compared to PNO-Mel (Fig. 4C). We also observed higher production of the inflammatory cytokines TNF-α (Fig. 4D) and IL-6 (Fig. 4E) in the PNO-Mel

samples when compared to PNO samples. Our results also revealed higher production of both TNF-α and IL-6 in PNO-Mel organoids with microglia when compared to PNO-Mel organoids without microglia, as expected. The presence of more apparent IBA1-positive microglia and the higher production of inflammatory cytokines in PNOs could be attributed to the activation of the microglia induced by the melanoma cells.

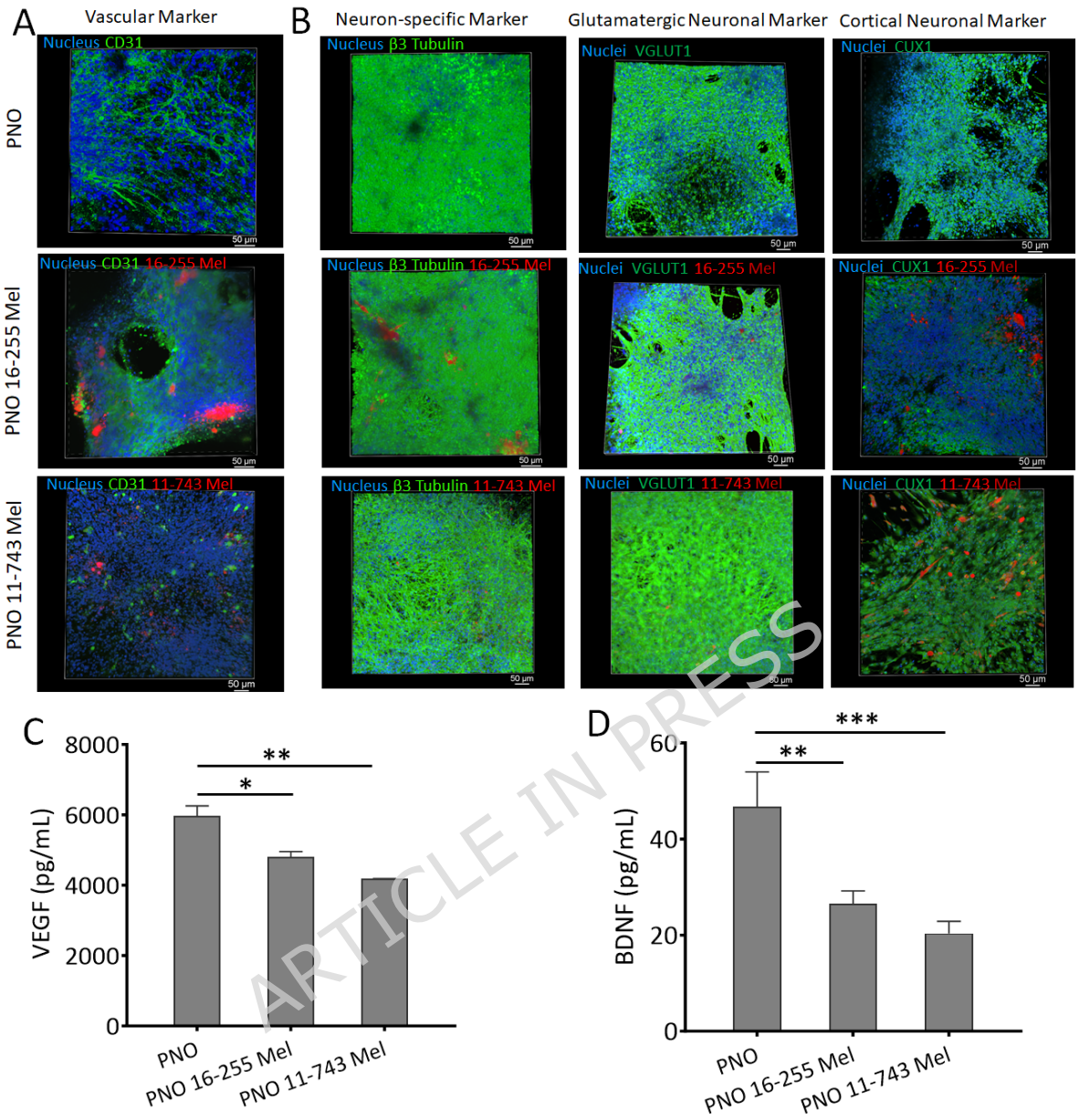

Fig. 3. Characterization of neuro-vascular marker proteins in the planar neural organoids. (A) Immunofluorescence staining of day 28 of neural organoids with antibodies against CD31 vascular marker protein (green) Scale bar 50 µm; (B) Immunofluorescence staining of day 28 of neural organoids with antibodies against β3-Tubulin, VGLUT1 and CUX1 neuronal markers (green). Scale bar 50 µm; (C) Measurement of VEGF protein produced by the day 28 neural organoids with or without melanoma cells; (D)

Measurement of BDNF protein produced by the day 28 neural organoids with or without melanoma cells. (*p < 0.05; **p < 0.01; ***p < 0.001).

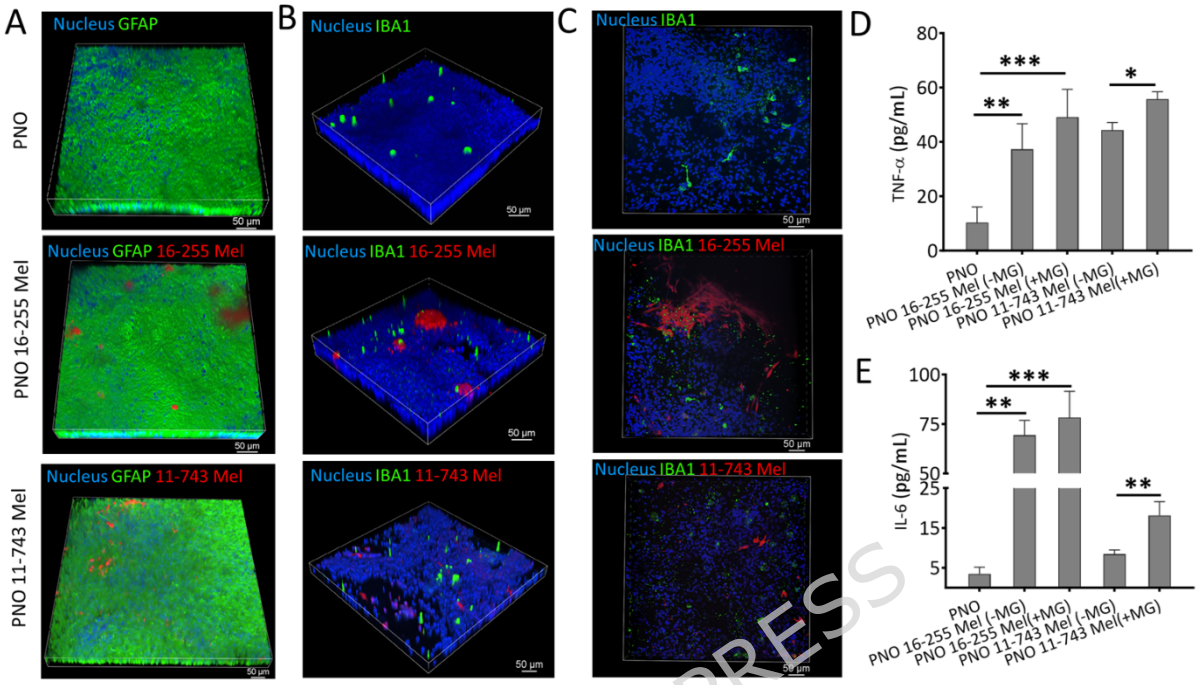

Fig. 4. Characterization of astrocyte and microglia-like phenotypes within the planar neural organoids. Immunofluorescence staining of day 28 of neural organoids with antibodies against (A) GFAP (green) and (B-C) microglia cell marker protein IBA1 (green). (D-E) Measurement of TNF-α and IL-6 protein from the culture of the different PNO conditions at day 28 (*p<0.05; **p < 0.01; ***p < 0.001).

Mass spectrometry-based proteomics analysis of planar neural organoids

Mass spectrometry-based proteomics analysis revealed a higher abundance of melanoma marker proteins in PNO-16-255 Mel when compared to PNO. The proteomic data analysis revealed 3214 proteins in the PNO-Mel and 3054 proteins in the PNO (Fig. 5A). Among these, 2949 proteins were common to both organoid types, 105 proteins were exclusively present in PNO, and 265 proteins were exclusively present in PNO-16-255 Mel (Fig. 5A). The volcano

plot illustrates fold change of all the common proteins expressed in both the PNO-Mel and PNO. Notably, the proteomics data showed substantial down-regulation of both the neurite outgrowth protein LSAMP and endothelial cell proliferation protein OGN in the PNO-Mel when compared to the PNO (Fig. 5B). The proteomics data also revealed higher expression of the cancer cell marker CDK1, melanoma marker proteins (GPNMB, GPM6B and MCAM) (Fig. 5C), and inflammatory cytokines (ILF2 and ILF3) (Fig. 5D) in the PNO-Mel when compared to the PNO. These results suggest that melanoma cell growth may impact neuro-vascular and melanoma marker proteins in the PNO.

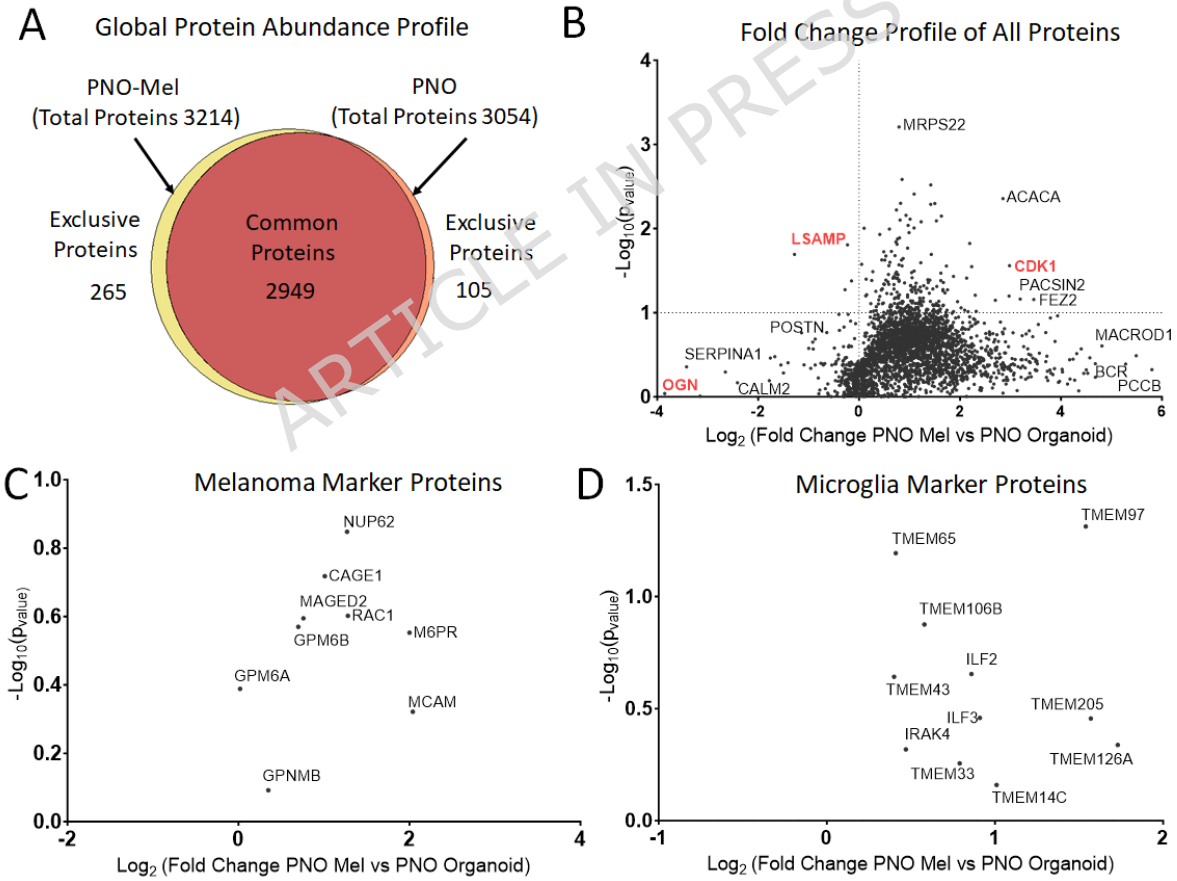

Fig. 5. Mass spectrometry-based proteomics analysis of lysate protein samples of the day 28 PNO and PNO-16-255 Mel organoids. (A) Global protein abundance in the PNO-16-255 Mel vs. PNO. (B) Fold change of expression of all the common proteins in the PNO-16-255 Mel vs. PNO. (C) Fold change of expression of a subset of melanoma marker proteins in the PNO-16-255 Mel vs. PNO. (D) Fold change of expression of microglia marker proteins in the PNO-16-255 Mel vs. PNO.

Effects of drug treatment on melanoma growth in the planar neural organoids

Treatment with clinically used melanoma inhibitors reduced the growth of the melanoma cell population in the organoids. Patient-derived mCherry-labeled BRAF V600E 16-255 and wild-type 11-743 melanoma cells were added to the PNOs on day 14. Confocal images showed the growth of these melanoma cells at day 28 on both a conventional plastic surface (2D culture) and in PNOs (3D culture) (Fig. 6A-B, Fig. 7A-B, Fig. S5-S6). Growth of both the 16-255 and 11-743 melanoma cell populations was monitored by measuring the mean fluorescence intensity of mCherry-labeled melanoma cells in the organoids (Fig. S7). Fluorescence area of the melanoma cells on the 2D plastic surface was over 5-fold greater than that in 3D PNO surfaces (Fig. 6C, Fig 7C). This could be due to the presence of a more complex physiological environment in the PNOs, including microglia that could potentially inhibit the growth of melanoma cells, as observed in previous studies. [49]

We next investigated the effects of two clinically used anti-cancer drugs DAB and TRA on the growth of the melanoma cells in the organoids. These drugs act to inhibit the growth of melanoma cells and DAB is particularly useful to treat metastatic melanoma cells with the BRAF V600E mutation, like the 16-255 melanoma cell line evaluated here.[50] PNO-Mel organoids were treated with 2 nM DAB or TRA every day from day 21 to day 28 of the culture. Drug treatment slowed the growth of the melanoma cells in comparison to the non-treated PNO-Mel (Fig. 6C, Fig. 7C and Fig. S7). Treatment with DAB and TRA also decreased the production of the metastatic melanoma marker protein GPNMB (Fig. 6D, Fig. 7D) and the inflammatory cytokine TNFα (Fig. 6E, Fig. 7E) in PNO-Mel samples when compared to that observed for the DMSO control-treated melanoma cells in the PNOs.

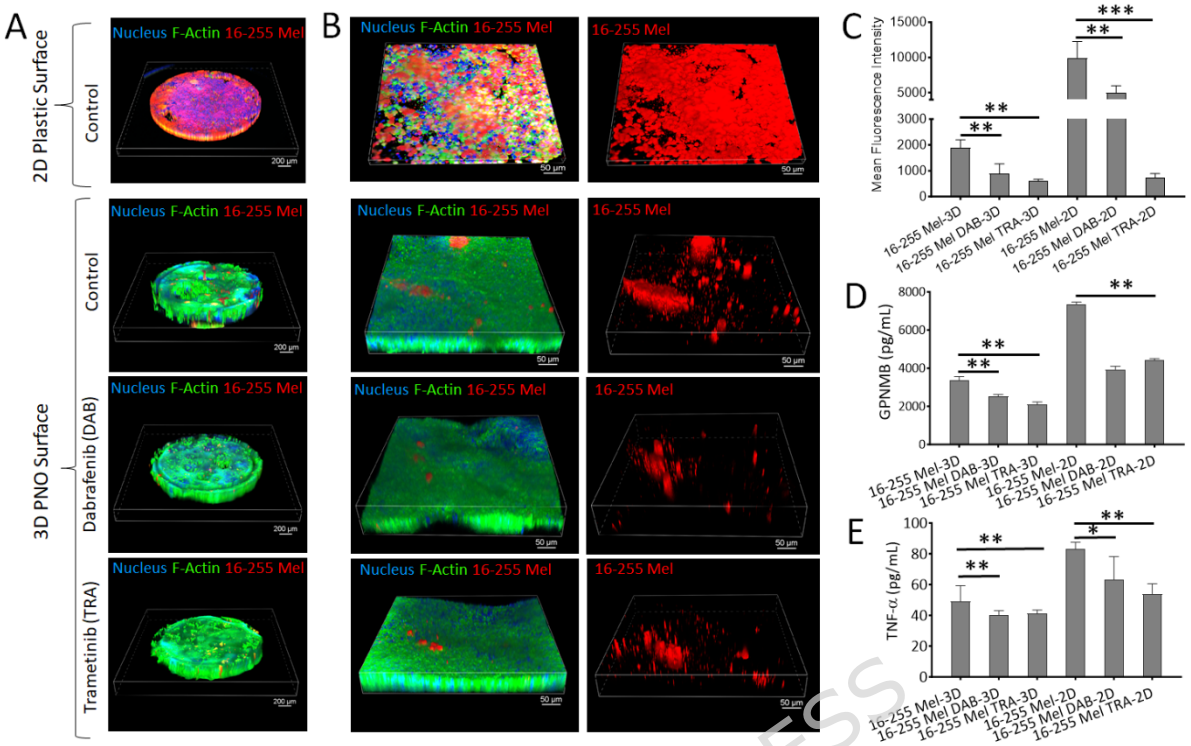

Fig. 6. Evaluation of anti-cancer drug treatment on the growth of the melanoma cells in the day 28 PNOs. (A-B) The effect of anti-cancer drug treatments on the growth of the patient-derived mCherry-positive 16-255 melanoma cells in both 2D culture and 3D culture (day 28). (C) Growth profile of the mCherry-positive 16-255 melanoma cells in the presence of drug treatments. (D) Measurement of the melanoma metastatic marker protein GPNMB in the presence of drug treatments. (E) Measurement of the anti-inflammatory cytokine TNF-α in the presence of drug treatments (* indicates $p<0.05$;**$p < 0.01$; ***$p < 0.001$).

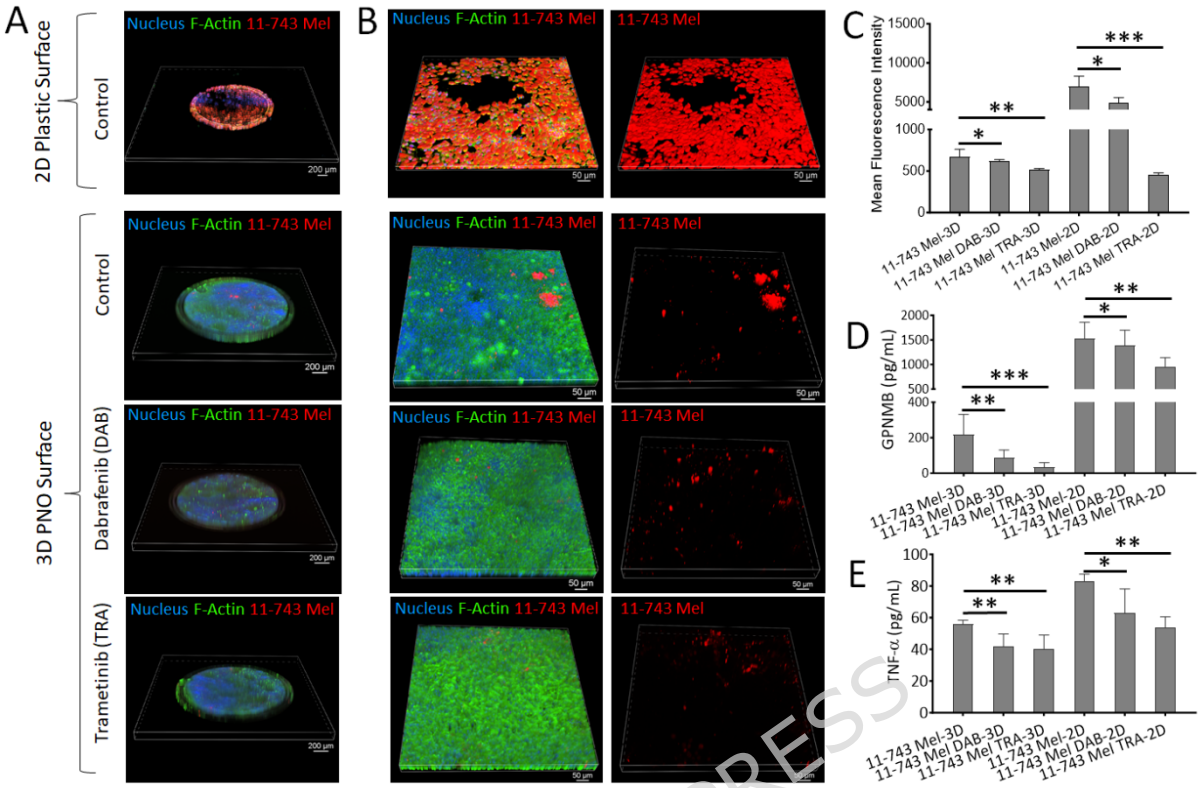

Fig. 7. Evaluation of anti-cancer drug treatment on the growth of the metastasized melanoma cells in the day 28 PNOs. (A-B) The effect of anti-cancer drug treatments on the growth of the patient-derived mCherry-positive 11-743 melanoma cells in both 2D culture and 3D culture. (C) Growth profile of the mCherry-positive 11-743 melanoma cells in the presence of drug treatments. (D) Measurement of the melanoma metastatic marker protein GPNMB in the presence of drug treatments. (E) Measurement of the anti-inflammatory cytokine TNF-α in the presence of drug treatments. (* indicates $p<0.05$; **$p < 0.01$; ***$p < 0.001$).

Notably, melanoma growth in PNOs showed some similarities to melanoma growth in patient-derived xenograft (PDX) models explored in previous studies. [51] Our results showed a two-fold growth of the 16-255 melanoma cell

population between day 7 and day 14 after their addition to the PNOs (Supporting Fig. S7B). In a recent study, Nemati *et al.* reported a similar growth profile of the melanoma cells in the PDX model, with a 2-fold growth of the melanoma from day 7 to day 14. [51] We also observed a 5-fold increase in the growth of 16-255 melanoma cells on a 2D plastic surface in contrast to their growth in a 3D PNO system. Taken together, these results show that the growth profile of the melanoma cells in PNOs had some similarity to melanoma growth in a physiologically relevant PDX model, [51, 52] whereas melanoma growth on the 2D plastic surface was substantially different.

Conclusion

Using human induced pluripotent stem cells (iPSCs), we engineered an *in vitro* 3D planar neural organoid model to study metastatic melanoma cells, including the effects of anti-cancer drug treatment on the melanoma growth. The PNOs showed characteristic neural and vascular signals, and cellular organization into 3D networks. This work demonstrated time efficient generation of PNOs only in 4 weeks of culture, and their scalability in 96 well plate as compared to generation of the traditional suspension culture organoids[53] which require much longer period of culture and expansion of tissues. Patient-derived melanoma cell lines incorporated and grew within PNOs, with growth characteristics that showed some similarity to previously observed melanoma growth in physiological PDX models. The presence of melanoma cells negatively impacted neurovascular tissue assembly and growth factor production in the PNOs, but increased the production of

microglia-associated neuroinflammatory cytokines. Treatment with the clinically used anti-cancer agents Dabrafenib and Trametinib decreased the growth of the melanoma cell population and lowered the levels of the metastatic melanoma marker protein GPNMB and the inflammatory cytokine TNFα in PNO-Mel as compared to that observed for the DMSO control-treated melanoma cells in the corresponding PNOs. Taken together, our results demonstrated that the PNOs may provide a useful human context to study the biology associated with metastatic melanoma growth, and may ultimately be adaptable to study other metastatic brain cancers.

Methods

All methods were approved by the by the Institutional Biosafety Committee (IBC) (B00000255) and the Stem Cell Research Oversight (SCRO) Committee (SC-2015-0029) at the University of Wisconsin-Madison, WI, USA. All methods were carried out in accordance with relevant guidelines and regulations. An informed consent was obtained from all subjects and/or their legal guardian(s) in the study.

1. Cell Culture

Human Induced Pluripotent Stem Cells (iPSCs)

WTC11 human iPSCs were grown on Matrigel (Corning #354277) coated six-well plate in Essential 8 (E8) medium supplemented with 10µM Rock inhibitor (R&D Systems #1254). E8 supplement (Fisher #A1517001) was added to E8 base media (Fisher #A1517001) in a 1:50 ratio to make the complete E8 media. Differentiation of WTC11 human iPSCs into endothelial cells (ECs),

pericyte cells (PC), neural progenitor cells (NPCs), and microglia (MG) was done as per our previously published protocol. [47, 54]

Patient-derived Melanoma Cells

Patient derived BRAF V600E mutation containing 16-255 melanoma and wild-type 11-743 melanoma cells were cultured on top of the planar neural organoids. 16-255 melanoma cells were derived from fibroblasts of a patient's small intestine and 11-743 melanoma cells were derived from cutaneous melanoma from a patient's chest wall.

Cell Resource:

Human iPSC line WTC-11 (Catalog # GM25256) was obtained from the Coriell Institute for Medical Research, NJ, USA. WTC11-EC, WTC11-PC, WTC11-NPC, and WTC11-MG cells were differentiated from the parent WTC11 iPSC line following our previously published protocol.[47] Patient-derived 16-255 and 11-743 melanoma cell lines were obtained from 'The University of Pittsburgh Cancer Institute Melanoma Tissue Bank and Melanoma Center Laboratory'. We performed routine mycoplasma testing to check the contamination in the cell lines, and no contamination was found in any of the cell lines used in this study. All the cell lines were contamination-free.

2. Preparation of PEG Hydrogels

Polyethylene glycol (PEG) hydrogels were prepared following our previously published procedure.[46] First, a sterile stock solution of '8-arm PEG

norbornene (tripentaerythritol)' (JenKem Technology, USA, Cat. # A10037-10), degradable peptide ‚Tryp-MMP' (Genscript, amino acid sequence KCGGPQGIWGQGCK), cell adhesion peptide 'CRGDS' (Genscript), and photoinitiator I2959 – Irgacure D2959 (Sigma #410896) were prepared in 1X PBS. Next, an appropriate volume of 8-arm PEG-norbornene (40 mg/mL), Tryp-MMP (60% molar ratio relative to norbornene arms), and CRGDS peptide (2 mM) were mixed, and the resulting mixture was placed on ice for 5 minutes. This resulting PEG-MMP-CRGDS solution was mixed with an equal volume of 0.2% ice-cold photoinitiator I2959. 10 µl of this gel mixture was added to each well of 96 96-well angiogenesis plate, which was then placed under a UV lamp for 5 minutes for hydrogel formation. Finally, 50 µl of DME/F-12 media (HyClone #SH3002301) was added on top of the hydrogels and incubated overnight for swelling and equilibration.

3. Generation of Planar Neural Organoids

First, 2 x 10^4 WTC11-EC cells and 4 x 10^3 WTC11-PC cells were seeded onto PEG hydrogels with a final volume of 50µL in E7V media. Cells were fed with 50µL of fresh E7V medium daily for 7 days. Next, 2.5 x 10^4 WTC11-NPC cells were added on day 7 using 50µL of N2B27(NG) culture media, and the organoids were treated daily with 50µL of fresh N2B27(NG) culture media. Next, only 625 numbers of WTC11-MG cells were added on day 12 in each organoid using 50µL of N2B27(NG) culture media. On day 14, 500 patient-derived mCherry-positive 16-255 melanoma and 11-743 melanoma cells were added on top of the planar neural organoids. Finally, the neural organoids

were treated with 2 nM concentration of clinical drugs Dabrafenib and Trametinib separately daily starting on day 21, and the culture of the organoids was continued till day 28.

4. Immunofluorescence Imaging

Planar neural organoid samples were washed with PBS and fixed directly on angiogenesis plates with 4% PFA at room temperature for 4 hours. Next, PNOs were permeabilized for 15 minutes in PBS buffer containing 25% methanol and blocked for 4 hours at room temperature in PBS buffer containing 10% normal donkey serum, 1% bovine serum albumin and 0.25% Triton X-100. PNOs were subsequently incubated overnight at 4 °C with the primary antibodies at 1:50 dilutions using PBS buffer containing 1% normal donkey serum, 1% bovine serum albumin and 0.25% Triton X-100. The samples were washed thrice with PBS-T buffer containing 0.05% Tween 20 and incubated with the corresponding secondary antibodies in PBS buffer containing 1% normal donkey serum, 1% bovine serum albumin and 0.25% Triton X-100 at 1:100 dilutions for 4 hours at room temperature. Finally, the stained PNO samples were washed five times with PBS-T buffer, and immunofluorescence images were acquired using a Nikon A1RS confocal microscope.

5. ELISA Assays

ELISA assays were performed using the organoid culture samples as per the vendor's protocol. Human VEGF Quantikine ELISA Kit (R&D Systems Cat#

DVE00); Human IL-6 Quantikine ELISA Kit (R&D Systems Cat# D6050); Human TNF-alpha Quantikine ELISA Kit (R&D Systems Cat # DTA00D) and Human BDNF ELISA Kit (Sigma Aldrich Cat# RAB0026) were used to measure the secreted proteins in the organoid culture.

6. Lysate Sample Preparation from Planar Neural Organoids

Planar neural organoids were washed twice with 1X PBS and treated with 50 µl of RIPA lysis buffer supplemented with 1X protease inhibitor cocktail for 4 hours on ice. Next, the lysate samples were collected by gentle pipetting and transferred to a microcentrifuge tube. Finally, samples were centrifuged at 10,000 × g for 10 minutes at 4 °C and the lysate samples were collected and analyzed for mass-spectrometry-based proteomic studies.

7. Proteomics Data Collection and Analysis

Enzymatic "In Liquid" Digestion

100 µl of PNO lysate sample was mixed with 100 µl of Milli-Q water and 800 µl of methanol, then vortexed to extract the proteins. Next, 200 µl of chloroform was added to delipidate, and finally, 600 µl of water was added to initiate phase separation. The upper phase was discarded, and the chloroform-containing lower phase was subsequently removed with methanol washes twice (vortexing and a 4-minute spin at maximum speed each round) at room temperature, followed by a final acetone wash of the protein pellet fraction. Pellets were solubilized in 20 µl of 8 M Urea in 25 mM NH_4HCO_3

(pH 8.5), and 5 µl was taken for the BCA assay. Next, 20 µg of protein per sample was used for tryptic/LysC digestion, where the samples were first diluted to a final volume of 60 µl with 2.5 µl of 25 mM DTT and 42.5 µl of 25 mM NH_4HCO_3 (pH 8.5) for the reduction step, which was carried out for 15 minutes at 56 °C. Then, 3 µl of 55 mM chloroacetamide was added for alkylation, and the samples were incubated in the dark at room temperature for 15 minutes. Next, the alkylation reaction was quenched by adding 8µl of 25mM DTT, followed by the addition of Trypsin/LysC solution [100 ng/µl 1:1 Trypsin (Promega): LysC (Fuji Film) mixed in 25 mM NH_4HCO_3] with an enzyme:substrate ratio 25:1 to the samples for a final volume 100µl. Digests were carried out overnight at 37 °C, then subsequently terminated by acidification with 2.5% trifluoroacetic acid to 0.3% final.

NanoLC-MS/MS

Protein digests were desalted using Pierce™ C18 SPE pipette tips (100 µl volume) as per the manufacturer's protocol; eluted in 20 µl of 70/30/0.1% of ACN/H_2O/TFA, and dried to completion in the speed-vac, and finally reconstituted to 1 µg/µl final concentration in 0.1% formic acid. Peptides were analyzed via NanoLC-MS/MS with the Agilent 1100 nanoflow system (Agilent), linked to a hybrid linear ion trap-orbitrap mass spectrometer (LTQ-Orbitrap Elite™, Thermo Fisher Scientific) and equipped with an EASY-Spray™ electrospray source (held at constant 35°C). Chromatography of peptides (prior to the mass spectral analysis) was accomplished using a capillary emitter column (PepMap® C18, 3 µM, 100Å, 150x0.075mm, Thermo Fisher

Scientific) onto which 2 µl of extracted peptides was automatically loaded. The mobile phase containing solvents A: 0.1% (v/v) formic acid , and B: 99.9% (v/v) acetonitrile, 0.1% (v/v) formic acid was used at flow speed 0.50 µL/min to load the peptides (over 30 minutes) and 0.3 µl/min to elute peptides directly into the nano-electrospray with gradual gradient from 0% (v/v) B to 30% (v/v) B over 280 minutes followed by rapid gradient from 30% to 50% (v/v) B over 10 minutes and concluded with 7 minute flush-out from 50% B to 95% (v/v) B at which time a 2 minute column conditioning at 95% (v/v) B took place. As peptides eluted from the HPLC column/electrospray source survey, MS scans were acquired in the Orbitrap with a resolution of 120,000 followed by CID-type MS/MS fragmentation in the LTQ Ion Trap of the 30 most intense peptides detected in the MS1 scan from 350 to 1800 m/z; redundancy was limited by dynamic exclusion.

Proteomics Data Analysis

All the experiments were performed in three biological replicates. T-test and two-way ANOVA test were performed for the comparison between the biological replicates (Supporting Fig. S8). The differential protein abundance was defined with P-value 0.05 and fold change ratio value 1. The acquired MS/MS data was analyzed using ‘Proteome Discoverer (ver. 3.1.0.638) Sequest HT’ search engine and Percolator validation against Homo sapiens reference database (UP000005640, 03/08/2024 download, 82,602 total entries) along with a cRAP common lab contaminant database (116 total entries). Static cysteine carbamido-methylation, and variable methionine

oxidation plus asparagine and glutamine deamidation, 2 tryptic miss-cleavages and peptide mass tolerances were set at 10 ppm with fragment mass selected at 0.6 Da. Peptide and protein identifications were accepted under strict 1% FDR cut-offs with high confidence XCorr thresholds of 1.9 for z=2 and 2.3 for z=3. Strict principles of parsimony were applied for protein grouping. Chromatograms were aligned for mapping the features of the proteins, and ion intensities were used for the quantification of precursor ions using unique and razor peptides. Signal intensities were normalized based on total peptide amount, and protein abundance calculations were based on summed peptide abundances. ANOVA (individual proteins) hypothesis testing was executed, and no imputation mode was applied.

8. Statistical Analysis.

All the experiments were performed in three biological replicates, and the results are reported as means ± SD. A two-way ANOVA test was used to analyze the statistical significance between data sets. Statistical significance has been represented as *p < 0.05, **p < 0.01, ***p < 0.001, and ****p < 0.0001.

Acknowledgements

We would like to thank ‘The University of Pittsburgh Cancer Institute Melanoma Tissue Bank and Melanoma Center Laboratory’ for providing us with the patient derived 16-255 and 11-743 melanoma cell lines.

Ethics declarations

Competing interest

The corresponding author is responsible for submitting a competing interest statement on behalf of all authors of the paper. The author(s) declare the following potential conflicts of interest with respect to the research, authorship, and/or publication of this article: W. L. Murphy and C. S. Lebakken are co-founders and shareholders in Stem Pharm, Inc., which is focused on commercial applications of neural organoids. All the remaining authors declare no conflict of interest.

Study approval statement

All methods were approved by the by the Institutional Biosafety Committee (IBC) (B00000255) and the Stem Cell Research Oversight (SCRO) Committee (SC-2015-0029) at the University of Wisconsin-Madison, WI, USA. All methods were carried out in accordance with relevant guidelines and regulations.

Consent to participate

An informed consent was obtained from all subjects and/or their legal guardian(s) in the study.

Author Contributions

W.L.M. conceptualized and secured funding for the project; J.M., E.E.T. and P.F.F. conducted the major experiment(s); A.R., U.M., G.S. and C.S.L. conducted additional experiments; J.M. wrote the original draft of the paper; All authors reviewed the manuscript.

Data availability

Proteomics data is provided within the manuscript or supplementary information files. Other datasets used and/or analyzed during the current study are available from the corresponding author upon reasonable request.

Supporting information

Electronic supplementary materials including proteomics data.

Additional information

Correspondence and requests for materials should be addressed to W. L. Murphy.

Publisher's note

Springer Nature remains neutral with regard to jurisdictional claims in published maps and institutional affiliations.

Funding

This research was funded by the US Environmental Protection Agency (STAR Grant no. 83573701), the US National Institutes of Health (award nos 1U01TR002383, R01HL093282 and 1R01NS109427, 1R43ES029898 and 1R43ES029897) and the US National Science Foundation (award nos EEC1648035 and DMR 170179).

References

1. Guan, X. Cancer metastases: challenges and opportunities. *Acta Pharm. Sin B.* **5** (5), 402-18 (2015).

2. Dillekas, H., Rogers, M. S. & Straume, O. Are 90% of deaths from cancer caused by metastases? *Cancer Med.* **8** (12), 5574-6 (2019).

3. Hutton, D., Kanodia, A. K., El-Maddawi, I., Hannah, L. & Hossain-Ibrahim, K. An update on current and emerging therapies for brain metastases. *Neurology & Neurotherapy Open Access Journal.* **5** (2), 1-6 (2020).

4. Fomchenko, E. I. & Holland, E. C. Mouse models of brain tumors and their applications in preclinical trials. *Clin Cancer Res.* **12** (18), 5288-97 (2006).

5. Fan, Y., Nguyen, D. T., Akay, Y., Xu, F. & Akay, M. Engineering a brain cancer chip for high-throughput drug screening. *Sci. Rep.* **6**, 25062 (2016).

6. Yamada, K. M. & Cukierman, E. Modeling tissue morphogenesis and cancer in 3D. *Cell.* **130** (4), 601-10 (2007).

7. Pampaloni, F., Reynaud E. G. & Stelzer E. H. K. The third dimension bridges the gap between cell culture and live tissue. *Nat Rev Mol Cell Biol.* **10**, 839-45 (2007).

8. Baker, B. M. & Chen, C. S. Deconstructing the third dimension: how 3D culture microenvironments alter cellular cues. *J Cell Sci.* **125**(Pt 13), 3015-24 (2012).

9. Hickman, J. A. et al. Three-dimensional models of cancer for pharmacology and cancer cell biology: capturing tumor complexity in vitro/ex vivo. *Biotechnol J.* **9** (9), 1115-28 (2014).

10. De Witt Hamer, P. C. et al. The genomic profile of human malignant glioma is altered early in primary cell culture and preserved in spheroids. *Oncogene.* **27** (14), 2091-6 (2008).

11. Bristow, R. G. & Hill, R. P. Hypoxia and metabolism. Hypoxia, DNA repair and genetic instability. *Nat Rev Cancer.* **8** (3), 180-92 (2008).

12. Mikhailova, V., Gulaia, V., Tiasto, V., Rybtsov, S., Yatsunskaya, M. & Kagansky, A. Towards an advanced cell-based in vitro glioma model system. *AIMS Genet.* **5** (2), 91-112 (2018).

13. Torsvik, A. et al. U-251 revisited: genetic drift and phenotypic consequences of long-term cultures of glioblastoma cells. *Cancer Med.* **3** (4), 812-24 (2014).

14. Perlman, R. L. Mouse models of human disease: An evolutionary perspective. *Evol Med Public Health.* 170-6 (2016).

15. Lancaster, M. A. et al. Cerebral organoids model human brain development and microcephaly. *Nature.* **501** (7467):373-9 (2013).

16. Mansour, A. A. et al. An in vivo model of functional and vascularized human brain organoids. *Nat Biotechnol.* **36** (5):432-41 (2018).

17. Cui, K. et al. Brain organoid-on-chip system to study the effects of breast cancer derived exosomes on the neurodevelopment of brain. *Cell Regen.* **11** (1), 7 (2022).

18. Mason, J. O. & Price, D. J. Building brains in a dish: Prospects for growing cerebral organoids from stem cells. *Neuroscience.* **334**, 105-18 (2016).

19. Chiaradia, I. & Lancaster, M. A. Brain organoids for the study of human neurobiology at the interface of in vitro and in vivo. *Nat Neurosci.* **23** (12), 1496-508 (2020).

20. Kelava, I. & Lancaster, M. A. Dishing out mini-brains: Current progress and future prospects in brain organoid research. *Dev Biol.* **420** (2),199-209 (2016).

21. Barker, N. et al. Lgr5(+ve) stem cells drive self-renewal in the stomach and build long-lived gastric units in vitro. *Cell Stem Cell.* **6** (1), 25-36 (2010).

22. Pompaiah, M. & Bartfeld, S. Gastric Organoids: An emerging model system to study helicobacter pylori pathogenesis. *Curr Top Microbiol Immunol.* **400**, 149-68 (2017).

23. Zhang, M., Liu, Y. & Chen, Y. G. Generation of 3D human gastrointestinal organoids: principle and applications. *Cell Regen.* **9** (1), 6 (2020).

24. Eicher, A. K. et al. Functional human gastrointestinal organoids can be engineered from three primary germ layers derived separately from pluripotent stem cells. *Cell Stem Cell.* **29** (1), 36-51 e6 (2022).

25. Pang, M. J. et al. Gastric organoids: progress and remaining challenges. *Cell Mol Gastroenterol Hepatol.* **13** (1), 19-33 (2022).

26. Seidlitz, T., Koo, B. K. & Stange, D. E. Gastric organoids-an in vitro model system for the study of gastric development and road to personalized medicine. *Cell Death Differ.* **28** (1), 68-83 (2021).

27. Huch, M. et al. Unlimited in vitro expansion of adult bi-potent pancreas progenitors through the Lgr5/R-spondin axis. *EMBO J.* **32** (20), 2708-21 (2013).

28. Moreira, L., Bakir, B., Chatterji, P., Dantes, Z., Reichert, M. & Rustgi, A. K. Pancreas 3D organoids: current and future aspects as a research platform for personalized medicine in pancreatic cancer. *Cell Mol Gastroenterol Hepatol.* **5** (3), 289-98 (2018).

29. Georgakopoulos, N. et al. Long-term expansion, genomic stability and in vivo safety of adult human pancreas organoids. *BMC Dev Biol.* **20** (1):4 (2020).

30. Driehuis, E., Gracanin, A., Vries, R. G. J., Clevers, H. & Boj, S. F. Establishment of pancreatic organoids from normal tissue and tumors. *STAR Protoc.* **1**(3), 100192 (2020).

31. Koike, H. et al. Engineering human hepato-biliary-pancreatic organoids from pluripotent stem cells. *Nat Protoc.* **16** (2), 919-36 (2021).

32. Jung, P. et al. Isolation and in vitro expansion of human colonic stem cells. *Nat Med.* **17** (10), 1225-7 (2011).

33. d'Aldebert, E. et al. Characterization of human colon organoids from inflammatory bowel disease patients. *Front Cell Dev Biol.* **8**, 363 (2022).

34. Crespo, M. et al. Colonic organoids derived from human induced pluripotent stem cells for modeling colorectal cancer and drug testing. *Nat Med.* **23** (7), 878-84 (2017).

35. Michels, B. E. et al. Human colon organoids reveal distinct physiologic and oncogenic Wnt responses. *J Exp Med.* **216** (3), 704-20 (2019).

36. Huch, M. et al. In vitro expansion of single Lgr5+ liver stem cells induced by Wnt-driven regeneration. *Nature.* **494** (7436), 247-50 (2013).

37. Ye, S. et al. A chemically defined hydrogel for human liver organoid culture. *Adv Funct Mater.* **30** (48), 2000893 (2020).

38. Prior, N., Inacio, P. & Huch M. Liver organoids: from basic research to therapeutic applications. *Gut.* **68** (12), 2228-37 (2019).

39. Harrison, S. P., Baumgarten, S. F., Verma, R., Lunov, O., Dejneka, A. & Sullivan, G. J. Liver organoids: recent developments, limitations and potential. *Front Med (Lausanne).* **8**, 574047 (2021).

40. Lam D., Dan Y. Y., Chan Y. S. & Ng H. H. Emerging liver organoid platforms and technologies. *Cell Regen.* **10** (1), 27 (2021).

41. De Crignis, E. et al. Application of human liver organoids as a patient-derived primary model for HBV infection and related hepatocellular carcinoma. *Elife.* **10** (2021).

42. Guan, Y. et al. A human multi-lineage hepatic organoid model for liver fibrosis. *Nat Commun.* **12** (1), 6138 (2021).

43. Lewis-Israeli, Y. R., Wasserman, A. H. & Aguirre, A. Heart organoids and engineered heart tissues: novel tools for modeling human cardiac biology and disease. *Biomolecules.* **11** (9) (2021).

44. Pang, J. K. S., Ho, B. X., Chan, W. K. & Soh, B. S. Insights to heart development and cardiac disease models using pluripotent stem cell derived 3D organoids. *Front Cell Dev Biol.* **9**, 788955 (2021).

45. Qian, X, Song, H. & Ming, G. L. Brain organoids: advances, applications and challenges. *Development.* **146** (8) (2019).

46. Majumder, J. et al. Human induced pluripotent stem cell-derived planar neural organoids assembled on synthetic hydrogels. *J. Tissue Eng.* **15**, 1-16 (2024).

47. Schwartz, M. P. et al. Human pluripotent stem cell-derived neural constructs for predicting neural toxicity. *Proc Natl Acad Sci U S A.* **112**, 12516-21 (2015).

48. Barry, C. et al. Uniform neural tissue models produced on synthetic hydrogels using standard culture techniques. *Experimental Biology and Medicine.* **242** (17),1679-1689 (2017).

49. Rodriguez-Baena, F. J., Marquez-Galera, A., Ballesteros-Martinez, P., Castillo, A., Diaz, E., Moreno-Bueno, G., Lopez-Atalaya, J. P. & Sanchez-Laorden, B. Microglial reprogramming enhances antitumor immunity and immunotherapy response in melanoma brain metastases. *Cancer Cell.* S1535-6108(25)00026-1 (2025).

50. Robert C. et al. Improved overall survival in melanoma with combined dabrafenib and trametinib. *N. Engl. J. Med.* **372**, 30-39 (2015).

51. Nemati, F. et al. Patient derived xenografts (PDX) models as an avatar to assess personalized therapy options in uveal melanoma: a feasibility study. *Curr. Oncol.* **30**, 9090–9103 (2023).

52. Yan, C. et al. Generation of orthotopic patient-derived xenografts in humanized mice for evaluation of emerging targeted therapies and immunotherapy combinations for melanoma. *Cancers.* **15**, 3695 (2023).

53. Hirokawa, Y. et al. Low-viscosity matrix suspension culture enables scalable analysis of patient-derived organoids and tumoroids from the large intestine. *Commun Biol.* **4**, 1067 (2021).

54. Aisenbrey, E. A. et al. A protocol for rapid pericyte differentiation of human induced pluripotent stem cells. *STAR Protoc.* **2**, 100261 (2021).